Processing and Characterization of Stable, pH-Sensitive Layer-by-Layer Modified Colloidal Quantum Dots

Ashvin T. Nagaraja,[†] Aishwarya Sooresh,[‡] Kenith E. Meissner,[†,‡] and Michael J. McShane[†,‡,*]

[†]Department of Biomedical Engineering [‡]Materials Science and Engineering Program, Texas A&M University, College Station, Texas 77843, United States

ABSTRACT Quantum Dots (QDs) stabilized with dihydrolipoic acid (DHLA) were used as a template for layer-by-layer (LbL) modification to study the effect on the QD optical properties. We studied several different polyelectrolytes to determine that large quantities of monodisperse DHLA-QDs could only be obtained with the weak polyelectrolyte pair of poly(allylamine hydrochloride) (PAH) and poly(acrylic acid) (PAA). The key to this success was the development of a two-step method to split the LbL process into adsorption and centrifugation phases, which require different pH solutions for optimum success. Solution pH is highlighted as an important factor to achieve sufficient QD surface coverage and QD recovery during wash cycles. We optimized the process to scale up synthesis by introducing a solvent precipitation step before ultracentrifugation that, when coupled with the correct pH conditions, results in a mean QD recovery of 86−90% after three wash cycles. We found that adsorption of PAH had a negligible effect on the quantum yield and lifetime but an additional layer of PAA resulted in a substantial decrease in both quantum yield and lifetime that could not be recovered by the addition of more layers. The PAH coating provides a protective coating that extends DHLA-QDs stability, prevents photo-oxidation mediated aggregation, alleviates concerns over batch variability, and results in pH-dependent emission.

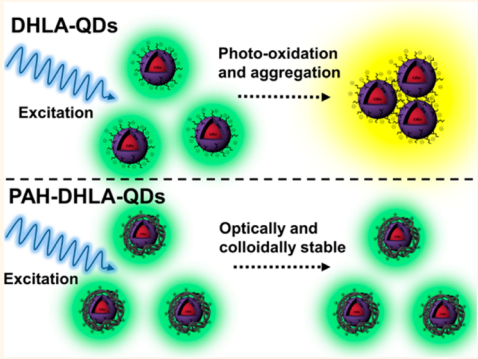

KEYWORDS: layer-by-layer · quantum dot · polyelectrolyte

Semiconductor nanocrystals or quantum dots (QDs) possess a number of unique properties that could enable them to revolutionize biomedical imaging and sensing.[1−3] The broad absorption spectrum of a QD sample increases toward the UV, allowing efficient excitation by any source with a wavelength shorter than the QD bandedge; thus, the excitation source can be spectrally separated from the emission, yielding a large effective Stokes shift. Because of quantum confinement effects, the optical properties are dependent on the size of the nanocrystal core. As the core gets larger, the optical properties (absorption bandedge and emission spectrum) shift to longer wavelengths. Size tunability allows a single material system to cover applications across a broad spectral region, tailoring the optical properties to the specific application. A key attractive feature of QDs for long-term sensing and imaging is high resistance to photobleaching, typically greater than an order of magnitude superior to conventional fluorescent dyes.[4,5] These properties make QDs ideal alternatives to organic dyes as donors in an energy transfer sensing scheme.[6−9]

Nanocrystalline quantum dots with narrow size distributions and desired optical properties are typically synthesized in nonpolar organic solvents and stabilized with hydrophobic ligands.[10] To ready QDs for use in biomedical applications, some modification and engineering of the QD surface is typically necessary. There are many routes to water solubilize QDs, with different methods having various tradeoffs between complexity, conditional stability, hydrodynamic size, and optical properties.[11−14] Mercaptocarboxylic ligands are commonly used because of the simple exchange process and resulting exposed carboxylic acid groups that provide for further functionalization. Short chain mercaptocarboxylic acid ligands offer the additional benefit of a resulting small hydrodynamic radius, which greatly improves efficiency for distance dependent

* Address correspondence to mcshane@tamu.edu.

Received for review April 24, 2013 and accepted June 19, 2013.

Published online June 20, 2013
10.1021/nn402061t

energy transfer. Commonly used short chain species include monothiolated molecules such as mercaptoproprionic acid (MPA), mercaptoacetic acid (MAA), or thioglycolic acid (TGA), but more recently the bidentate dihydrolipoic acid (DHLA)[15,16] has emerged as a more stable alternative because of the higher affinity of the dithiol compared to a monothiol. The high affinity of thiol ligands for metallic surfaces allows the hydrophilic molecule to spontaneously exchange with the more weakly bound hydrophobic trioctylphosphine oxide (TOPO) ligands, often used during synthesis.[17] However, the transfer to water is accompanied by a severe and variable decrease in quantum yield[15,18] with a colloidal stability that is susceptible to photooxidation mediated aggregation.[19]

In this work, we explored layer-by-layer (LbL) electrostatic self-assembly as a versatile method for surface modification of colloidal DHLA-stabilized QDs (DHLA-QDs). While LbL has been primarily applied to large, flat substrates,[20,21] a version of LbL was also developed for coating micrometer scale colloids.[22] However, applying LbL on nanoscale templates below 100 nm is not a trivial adaptation and has realized variable success on metals,[23−29] oxides,[30] polymeric particles[31] and QDs.[32,33] Both theoretical and experimental analyses have found that as particle size decreases, LbL becomes increasingly difficult due to the increasing nanoparticle surface curvature that encumbers complete wrapping by a rigid polyelectrolyte.[23,25,34,35] The importance of choosing the right conditions to prevent interparticle bridging and flocculation was first outlined by Caruso, with polystyrene[31] and 10−30 nm gold nanoparticles.[23] Utilizing the sensitivity of the plasmon band shift, Schneider *et al.* systematically vetted the parameters necessary for coating 13.5 nm gold nanoparticles.[26,27] A key finding of their work was the requirement for dilute mixing conditions for adding a low concentration of nanoparticles to an excess of polyelectrolyte to minimize aggregation and optimize particle recovery. A more in-depth look at the history of this topic is given in two recent reviews;[36,37] here, we will focus on the unique challenges and added considerations when extending this framework toward coating QDs.

The small size of QDs and the lower density compared to gold nanoparticles makes recovery of QDs and efficient separation of excess polyelectrolyte a significant challenge.[25,32] High speed centrifugation for long periods of time improves sedimentation, but under improper conditions leads to the formation of tightly packed pellets of irreversibly aggregated nanoparticles. Separation by any size-exclusion method (filtration, size exclusion chromatography, or dialysis) is virtually impossible, as particle circumference and polyelectrolyte chain length must be specifically chosen to be of similar size;[29] resulting in either polyelectrolyte retention or QD loss. Furthermore, a trade-off in volume and concentration exists: processing a large amount of dilute nanoparticles is both tedious and expensive, whereas high concentration of sample slows down the process and the excess polyelectrolyte clogs small pore-size filters.

It appears that the work on individual polyelectrolyte coated QDs is limited to two publications. Jaffar *et al.* used one bilayer of poly (allylamine hydrochloride) (PAH) and poly(vinylsulfonic acid) (PVSA) to invert the charge of MAA modified QDs for surface patterning.[33] This work showed the practicality of LbL on QDs but preceded the understanding provided by Schneider to provide the largest quantity of monodisperse LbL-coated QDs. Additionally, characterization of the effects of the polyelectrolyte on the optical properties was not an emphasis. Jin *et al.* used a lipid-PEG-COOH-stabilized QD followed by two bilayers of PAH and poly(sodium-4-styrenesulfonate) (PSS) as spacers for dual imaging modality plasmonic QDs. However, the method used for LbL was limited by the low recovery after each wash step even when ultracentrifugation was used.[32] It is also noteworthy that long-chain polyelectrolytes have been used to produce controlled aggregates as nanocapsules to mitigate QD toxicity[38] and to reverse the surface charge and adsorb negatively charged species for sensing applications.[39−41] However, the intent of these studies was not to produce monodisperse coated QDs, since the conditions used are known to induce flocculation. The resulting QDs were not characterized as monodisperse and were likely unusable as stable suspensions.

On the basis of this limited knowledge, the focus of this work was developing methods to coat and retain large quantities of monodisperse QDs by following the techniques outlined for gold nanoparticles. Preventing aggregation was a major consideration, as availability of individual modified QDs is important for many applications; however, preservation of the QD optical properties was the primary goal. The key to this is understanding how the optical properties, specifically the quantum yield and lifetime, are affected by the interaction of different polyelectrolytes with the mercaptocarboxylic acid modified QD surface.

RESULTS AND DISCUSSION

The basic LbL process is depicted in Scheme 1 where (A) QDs in chloroform are transferred into water by the addition of (B) DHLA, followed by adsorption of a (C) cationic polyelectrolyte and then an (D) anionic polyelectrolyte with wash cycles between each step. Polyelectrolytes were chosen based on the following criteria: low molecular weight, broad commercial availability, and previous success in coating nanoparticles of similar size and surface coating. It is well understood that polyelectrolytes should be low molecular weight in order to prevent interparticle bridging. The lower limit is less well-defined; theoretical modeling and experimental work has shown that polyelectrolyte

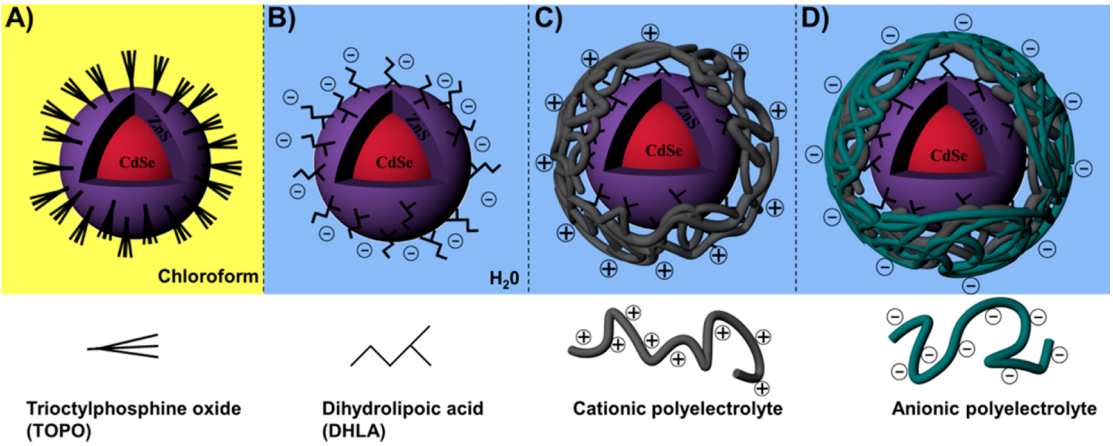

Scheme 1. (A) TOPO-QDs in chloroform; (B) anionic water-soluble DHLA-QDs; (C) cationic polyelectrolyte coated QDs; (D) anionic polyelectrolyte coated QDs

chain length should be approximately equivalent to particle circumference,[34,35] but this choice is greatly limited by commercial availability. For cationic polyelectrolytes, we chose to study 15 kDa poly(allylamine hydrochloride) (PAH), 1.8 kDa linear poly(ethylenimine) (PEI) and 8.5 kDa poly(diallyldimethylammonium chloride) (PDADMAC). For anionic polyelectrolytes, we chose 15 kDa poly(acrylic acid) (PAA), 8.5 kDa poly(sodium-4-styrenesulfonate) (PSS) and 4−6 kDa poly(vinylsulfonic acid) (PVSA).

When using either linear PEI or PVSA initial adsorption produced colloidally stable QDs, however, irreversible aggregation was observed after several wash steps. We believe that the nanoparticles are temporarily stabilized by the very low molecular polyelectrolyte acting similar to a surfactant, but the inability of the polyelectrolyte to effectively wrap the particle results in a weak electrostatic interaction that is disrupted after several wash steps. In contrast, strong polyelectrolytes such as PSS or PDADMAC result in particle flocculation due to incomplete surface coverage because of their inability to wrap the highly curved QD without increasing ionic strength (DHLA-QDs aggregate in the presence of even very low salt concentrations) or the polyelectrolyte acting as mortar to form bridges between neighboring QDs. Under all conditions studied, we were only able to produce colloidally stable and monodisperse QDs with one bilayer using the weak polyelectrolyte pair of PAH and PAA.

The DHLA ligand used to make QDs water-soluble imparts colloidal stability resulting from electrostatic repulsion of the acid groups, however, this only holds at a pH above the pI of the surface groups and under low ionic strength conditions, requiring storage and use in a buffer above pH 7.[16] Therefore, to effectively coat these anionic QDs with cationic PAH, the first adsorption step must occur above pH 7 and near or below the pK_a of PAH (8.5−9). We found that adsorption of the first layer of PAH at pH 8 or below resulted in substantial loss of QDs (sticking to the container surface) as well as complete aggregation during centrifugation. Increasing the adsorption pH to 8.1 or above increases the QD surface charge density while simultaneously decreasing the polyelectrolyte backbone charge density; producing coated QDs that no longer adhere to the container surface. The interplay of charge density between the QD and polyelectrolyte allows for (1) a higher grafting density or better surface coverage of the QD because of more effective wrapping by the weaker charged polyelectrolyte and/or (2) formation of a thicker coating by an increased the number of polyelectrolyte chains required to overcompensate for the highly charged QD. The resulting QDs are colloidally stable; however, subsequent centrifugation to remove excess polyelectrolyte causes formation of an irreversibly aggregated pellet. To overcome this problem, a two-step method was developed wherein PAH is first adsorbed to the QD at a pH between 8.1 and 9 to form a stable coating and then the pH is decreased below pH 8 before centrifugation. Increasing the surface charge density of the PAH coated QDs (PAH-DHLA-QDs) before centrifugation prevents pellet formation and aggregation. The strong electrostatic stability imparted by the polyelectrolyte coating as well as the small size and low density of the QD necessitates extended periods of high speed ultracentrifugation to efficiently remove the excess polyelectrolyte, while minimizing the number of wash steps and retaining the maximum amount of sample. Using this procedure, the coated QDs can be ultracentrifuged at 210 000 RCF for more than 12 h without visible pellet formation. Instead, the particles form loose sediment that is easily resuspended by a single pipet aspiration.

The dilute mixing conditions and large polyelectrolyte excess required to inhibit particle cross-linking and aggregation creates a tedious bottleneck for multiple wash steps. This was overcome by introducing a solvent precipitation and concentration step that precipitates both the QD and polyelectrolyte by lowering

the solution dielectric constant with the addition of excess isopropyl alcohol. After centrifugation at 10 000 RCF, the sediment mix can then be resuspended in a small amount of buffer, decreasing the volume 25:1 before ultracentrifugation. This first ultracentrifugation step needs to be longer in order to improve QD retention because the concentrated PAH becomes very viscous. The second and third wash cycles were shorter but varied depending on QD and polyelectrolyte concentrations. Using this procedure with an adsorption pH of 8.1 or pH 8.25−9 and a centrifugation pH of 7.2 in both cases, an average recovery rate of 76% and 86−90% was achieved, respectively, after the three wash steps were completed. This recovery rate is similar to what was found with 13.5 nm AuNPs[26] and much higher than the 30% recovery reported for similarly sized (5 nm) gold nanoparticles.[25] The process is repeated to add a layer of PAA but using a pH of 6−7.2 for adsorption and pH 8−8.5 for centrifugation.

Zeta potential measurements are reported in Figure 1 for DHLA-QDs (−38.6 ± 1.6 mV) in 5 mM pH 8 Tris buffer and full charge reversal for PAH-DHLA-QDs (+67 ± 7.08 mV) and PAA-PAH-DHLA-QDs (−51.5 ± 2.21 mV) in 5 mM pH 7.2 Tris buffer. The large magnitude of charge reversal of the PAH layer is higher than observed with MAA-QDs[33] or iron oxide coated with PAH[30] but similar to that found with gold nanoparticles.[26] One benefit of PAH-DHLA-QDs is the added stability at lower pH conditions. PAH is expected to be fully ionized below pH 7.5, and particles coated with PAH are both highly charged and stable; in contrast, DHLA-QDs aggregate as the solution becomes acidic.

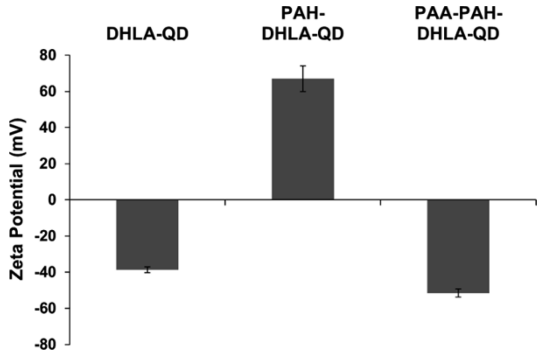

Figure 1. Zeta potential of the DHLA-QD in 5 mM Tris buffer pH 8, PAH-DHLA-QDs and PAA-PAH-DHLA-QDs in 5 mM Tris pH 7.2 (n = 3).

TEM was employed to assess aggregation states and morphology of the DHLA-QDs before and after coating with polyelectrolytes. TEM micrographs in Figure 2 show the (A) DHLA-QDs, (B) PAH-DHLA-QDs and (C) PAA-PAH-DHLA-QDs. It is clear from these micrographs that after coating with two polyelectrolyte layers the QDs are still well-defined with little to no visible aggregation.

Typical emission and absorption spectra are shown in Figure 3A and quantum yield relative to Rhodamine 6G in Figure 3B for DHLA-QDs (10.12%), PAH-DHLA-QDs (9.8 ± 0.6%) and PAA-PAH-DHLA-QDs (0.73 ± 0.1%).[42] There appears to be some increased scattering after the addition of polyelectrolyte, but there is no clear shift in the first exciton or emission peak. The adsorption of PAH has an insignificant effect on the quantum yield, while the addition of PAA is accompanied by a substantial decrease in quantum yield. We found the change in quantum yield after the addition of PAH was variable depending on the initial DHLA coating and the ZnS shell thickness. With a thinner ZnS shell the quantum yield would initially increase, but the addition of an anionic polyelectrolyte layer still resulted in a substantial decrease in quantum yield below that of the original DHLA-QDs (Figure S1). The quantum yield could not be recovered by the addition of more PAH. The strong quenching of QD luminescence observed in the presence of PAA was also observed for PVSA (Figure S1) and PSS (Figure S2); both of the latter also triggered aggregation (Figure S3). We attribute the quenching to a localized acidic environment created by the anionic polyelectrolytes causing quenching by the same mechanism that renders the DHLA-QDs pH sensitive. To gain further insight into the processes involved, we studied the change in the long and short luminescence lifetime components after the addition of each polyelectrolyte. The mean long lifetime component was 7.66 ± 0.47 ns for DHLA-QDs, 8.11 ± 0.49 ns for PAH-DHLA-QDs and 3.21 ± 0.36 ns

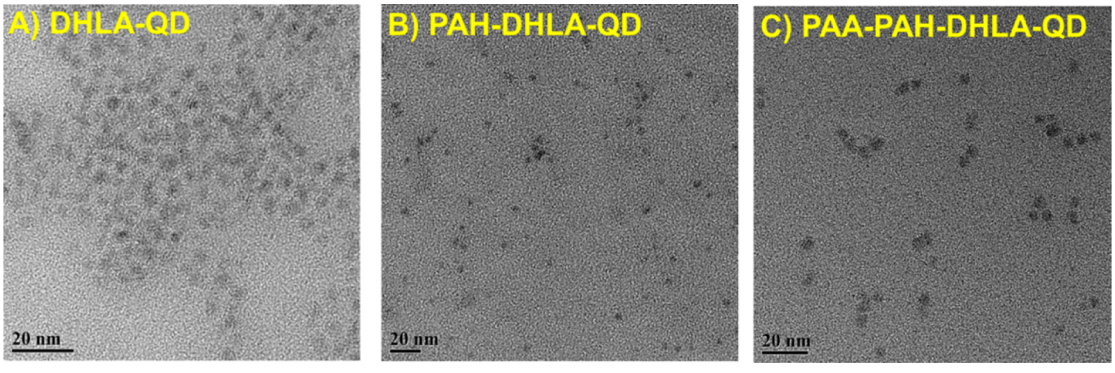

Figure 2. TEM images of (A) DHLA-QDs, (B) PAH-DHLA-QDs and (C) PAA-PAH-DHLA-QDs.

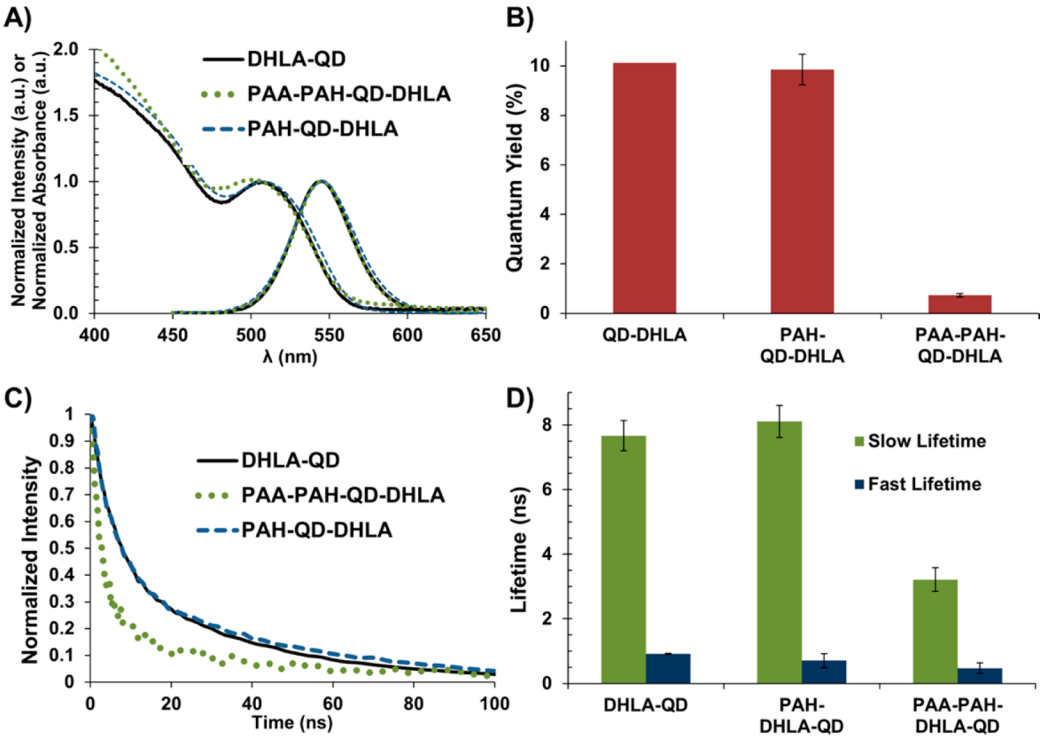

Figure 3. (A) Typical emission and absorbance spectra normalized to peak intensity and first exciton peak absorbance, respectively. (B) Quantum yield relative to Rhodamine 6G in water (one batch of DHLA-QD stock suspension, and $n = 3$ separate, parallel batches of coated QDs prepared from the same DHLA-QD stock). (C) Normalized raw luminescence lifetime. (D) Slow and fast lifetime component values ($n = 3$).

for PAA-PAH-DHLA-QDs (Figure 3C,D). The small lifetime component decreased after the addition of each layer, from 0.92 ± 0.02 ns for DHLA-QDs to 0.71 ± 0.22 ns and 0.47 ± 0.16 ns for PAH-DHLA-QDs and PAA-PAH-DHLA-QDs, respectively. The slow lifetime component showed no significant change after the addition of PAH but decreased extensively after the addition of PAA, indicating that PAA might be affecting the surface properties of the QD.[43] This is partially consistent with the findings of Rama *et al.*, when the effect of long-chain polyelectrolytes absorbed on MPA-QDs was studied a minimal effect on QD lifetime was observed for addition of both PAH and PSS.[41] Our results confirm their observations for PAH, but we observe a large decrease with the addition of the anionic polyelectrolyte. This could be attributed to our use of PAA instead of PSS or our LbL method providing more complete surface coverage of the second layer because we are maintaining monodisperse QDs. Based on the conditions used in their study we speculate that their methods produce agglomerates of QDs buried in the PAH, such that many of the QDs contributing to the optical measurements were unable to interact with the second layer of anionic polyelectrolyte.

Figure 4A illustrates the pH-dependent luminescence and stability of the PAH-DHLA-QDs in 50 mM Tris buffer between pH 3−9. As expected, above pH 8 we observe particle settling as the charge density of the PAH-DHLA-QD decreases. Below pH 8, the PAH-DHLA-QDs are colloidally stable. However, below pH 6 there was an irreversible blue shift in the emission (>20 nm), a change also observed with DHLA-QDs that we attribute to the stronger acidic conditions etching the QD surface or reducing the affinity of the ZnS overcoat. The pH-dependent intensity measurements of PAA-PAH-DHLA-QDs, PAH-DHLA-QDs and DHLA-QDs are presented in Figure 4B. Error bars for the intensity measurements represent triplicate measurements of the same sample taken 5 min apart, showing the stability of PAH-DHLA-QDs for repeated optical interrogation. The intensity of PAH-DHLA-QDs has a linear relationship with pH between pH 6.5 and 8 with a 15.9% change in luminescence for each 0.1 pH units. At pH 8.5 and above, the QDs settle out of solution, precluding accurate measurements. QD surface modification with mercaptocarboxylic acid ligands results in a reduction in overall quantum yield as well as a pH-dependent sensitivity based on protonation of the carboxylic acid group causing changes in trap states and electron−hole recombination.[44,45] This mechanism has been previously exploited several times to produce both photoluminescence intensity[45−47] and lifetime decay based pH sensors.[44] The PAH-DHLA-QDs retain this sensitivity to the surrounding environment although they exhibit a shift of the linear range toward higher pH. The PAA-PAH-DHLA-QDs are also colloidally stable over the pH range of 6−9. Compared

to PAH-DHLA-QDs, these exhibit an increase in luminescence intensity with increasing pH as well (Figure S4), but the magnitude of change is not significant compared to measurement error (Figure 4B).

Although it has been reported that DHLA-QDs are stable for 6−24 months,[6] we found that irreversible aggregation could be observed as quickly as a few days to weeks after production. It was observed that any exposure to light, including measurements of fluorescence or absorption, may initiate an avalanche of aggregation. This makes DHLA-QDs highly unsuitable for sensor applications, as each attempt to interrogate the system with light induces changes in optical properties and stability. When exposed to UV irradiation (100 W, 365 nm) for 30 min, the DHLA-QD emission shifted toward the red and subsequently aggregated, whereas PAH-DHLA-QDs exhibited no shift in emission spectrum or aggregation even after 3 h of UV irradiation (Figure 5A). Furthermore, even when refrigerated and protected from light, DHLA-QDs still eventually aggregate; in contrast, PAH-DHLA-QDs remain stable for at least an additional 8 months compared to the very same source batch of uncoated DHLA-QDs (Figure 5B). This implies that the PAH coating may ameliorate concerns over batch-to-batch variability and unknown long-term stability of DHLA-QDs by preventing pathways to aggregation.

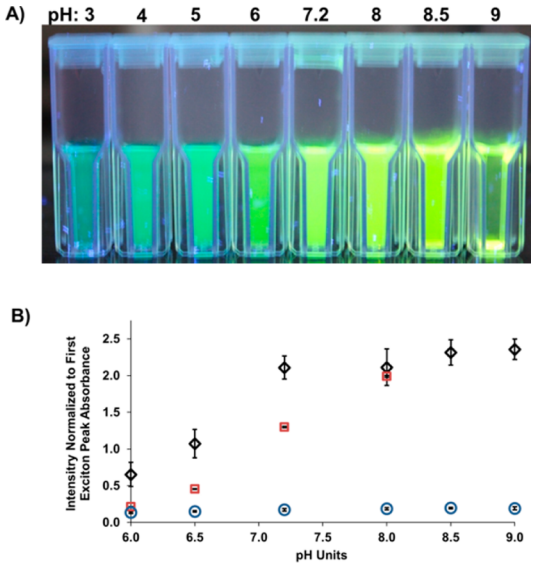

Figure 4. (A) Visual colloidal stability and luminescence intensity of PAH-DHLA-QDs in pH 3−9 Tris buffer under UV illumination. (B) Intensity measurements for different pH values normalized to the first exciton peak absorbance for DHLA-QDs (black ◊), PAH-DHLA-QDs (red □), and PAA-PAH-DHLA-QDs (blue ○).

CONCLUSIONS

This work expands on the applicable knowledge for colloidal LbL by taking into account solution pH as a crucial aspect when dealing with electrostatically stabilized nanoparticles and weak polyelectrolytes. Separation of the LbL process into two distinct phases provides more effective control of the charge density interplay between the QD and weak polyelectrolyte garnering a high recovery of monodisperse particles. The generality of the LbL process permits the use of these methods to coat a variety of other materials, which is especially important for low density nanoparticles of similar size which require ultracentrifugation for separation.

An interesting finding is that once the polyelectrolyte is adsorbed in a lower charge density state, a change in the pH to increase charge density does not induce complete desorption. Further study is necessary in order to precisely understand how variable solution pH affects polyelectrolyte grafting density and thickness during and after the adsorption phase. The PAH layer remains on the surface and provides a

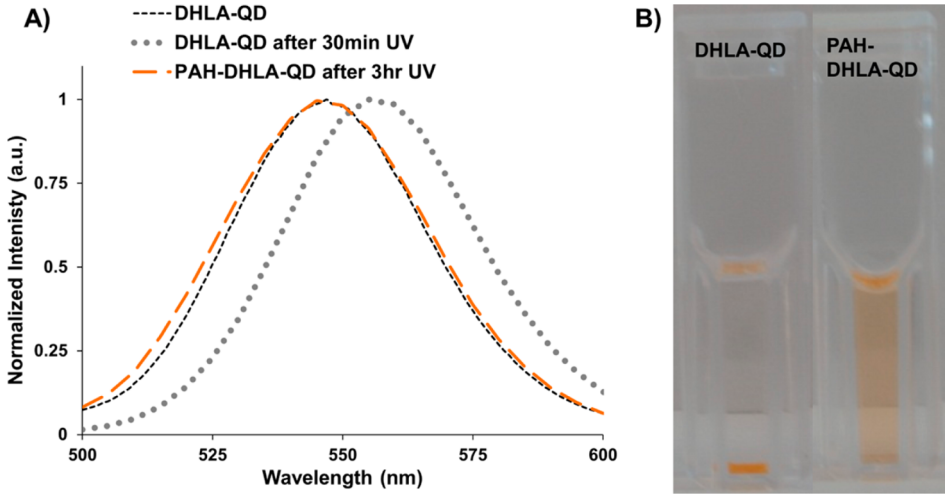

Figure 5. (A) Emission peak of DHLA-QDs and PAH-DHLA-QDs after 30 min and 3 h of UV exposure, respectively. (B) Visualization of colloidal stability of DHLA-QDs and PAH-DHLA-QDs after 8 months of storage under refrigeration in 50 mM pH 8 Tris buffer.

protective coating that overcomes batch-to-batch variability, affording superior long-term stability for storage. The ability to respond to changes in the local environment while withstanding repeated optical interrogation, makes PAH-DHLA-QDs a suitable alternative to DHLA-QDs for long-term sensing applications.

The low quantum yield of PAA-PAH-DHLA-QDs represents severe limitations for practical applications. Additionally, the PAA coating procedure could not be optimized since the QDs could not be incubated near the pK_a of PAA (~4.5) without degradation of the QD. We believe that the anionic polyelectrolyte quenching of QD luminescence would occur for any QD surface coating that imparts pH sensitivity. Future work will focus on alternative methods for water solubilizing QDs that provide surface passivation to prevent pH sensitivity and resistance to acidic degradation. Achieving this protective effect with sufficiently thin layers to preserve nanoscale energy transfer is a key challenge for advancing these materials.

METHODS

QD Synthesis. CdSe/ZnS core/shell QDs were synthesized according to previously reported procedures.[10,48,49] The synthesis was carried out in a single mode CEM Discover microwave reactor operating at 300 W, 2.45 GHz. In a typical experiment, cadmium oxide (CdO, 99.99%, Alfa Aesar, 0.0514 g, 0.4 mM), tetradecylphosphonic acid (TDPA,98%, Alfa Aesar, 0.2232 g, 0.8 mM) and TOPO (3.7768, 9 mM) were heated with continuous stirring in a 50 mL glass flask. The mixture was heated to ~300 °C under argon (Ar) flow (~1 mL/s) for 35 min. To this mixture, a selenium stock solution (0.0411 g, 0.5 mM, Aldrich, 99%) dissolved in 2.4 mL (2 g) of tri-*n*-octylphosphine (TOP, 99%, Aldrich) was injected at 270 °C and the reaction was continued for 4 min to allow the growth of the CdSe QD cores. This was followed by the addition of Zn and S precursors: 1.6 mL (12 mM) of dimethylzinc (DMZ, 1 M in heptane, Aldrich), 0.42 mL (2 mM) of hexamethyldisilathiane (HMDS, Aldrich), and 6.3 mL (14 mM) of TOP, for the ZnS shell formation. The reaction mixture was heated at 200 °C for 30 min.

DHLA Synthesis. DHLA was freshly prepared according to previously reported methods.[6] In a typical experiment, 4 g of (±)-α-lipoic acid (98%, Sigma) was reduced with a fresh stock of excess (3 g) sodium borohydride (NaBH4, 98%, Sigma). The reaction mixture was chilled to 4 °C and allowed to stir for 2 h under a constant argon blanket. It was then acidified with 15 mL of 12 M hydrochloric acid followed by the addition of ~100 mL of toluene. Pure DHLA was extracted from this mixture by evaporation using a rotovap leaving behind ~4 mL of DHLA. About 0.5 mL of pure DHLA was added to few hundred milligrams of QDs and heated at ~90 C on a hot plate with continuous stirring for 12 h. The resulting mixture was suspended in 3 mL of methanol followed by the addition of excess (approximately 1 g) potassium *tert*-butoxide (K-*t*BuO). The solution was centrifuged and the resulting DHLA-QDs were then suspended in Tris buffer pH 8−8.5. DHLA-QDs were filtered using a 0.2 μm syringe filter (Nalgene, PES 0.2 μm) and then a 30 kDa centrifuge filter in order to remove any excess K-*t*BuO in solution.

QD Characterization Techniques. Absorption spectra were recorded on a Hitachi U-4100 UV−vis-NIR spectrophotometer. Steady-state photoluminescence spectra were collected on a QuantaMaster 40 system by Photon Technology International (Ontario, Canada) with a 75 W continuous xenon arc lamp and digital PMT detection system using 1 nm excitation and emission slit widths, 1 s integration time. Fluorescence lifetime was collected using a TimeMaster LED system by Photon Technology International (Ontario, Canada) using a 405 nm LED (1.5 ns pulse width) for excitation and stroboscopic detection with 25 nm emission slit width, a 495 long pass filter, and sequential scanning with a logarithmic collection interval. Lifetime modeling was performed using the algorithm included in PTI's Felix32 software using a 3 exponential terms to fit the decay traces. The quality of fitting was determined by the reduced chi-squared method. QD samples were imaged using Transmission Electron Microscopy (TEM). TEM grids were glow discharged using PELCO easiGlow (Ted Pella, Inc., Redding,CA) in order to make the grid surface hydrophilic. Two microliters of solution was dropped on a 200 lines/in.^{2} mesh copper grids (Electron Microscopy Sciences, Hartfield, PA). Grids were analyzed on a FEI Tecnai G2 F20 at an accelerating voltage of 200 kV. Images were recorded using a Gatan CCD camera. Zeta potential was measured using a ZetaSizer Nano Series ZEN 3600 Spectrometer (Malvern Instruments Ltd., Malvern, Worcestershire, United Kingdom). The measurement was carried out with a concentration of 100 nmol/L of QDs in 5 mM Tris buffer.

Layer-by-Layer. Poly(allylaminehydrochloride) (PAH) M_w = 15 000 g·mol^{-1}(Sigma-Aldrich), linear poly(ethylenimine) (PEI) M_w = 1800 g·mol^{-1} (Sigma-Aldrich), poly(diallyldimethylammonium chloride) (PDADMAC) M_w = 8500 g·mol^{-1} (Polysciences), poly(sodium-4-styrenesulfonate) (PSS) M_w = 8500 g·mol^{-1} (Polysciences), poly(acrylic acid) (PAA) M_w = 15 000 g·mol^{-1} (Sigma-Aldrich), poly(vinylsulfonic acid) (PVSA) M_w = 4000−6000 g·mol^{-1} (Sigma-Aldrich). All polyelectrolytes were suspended in desired pH buffer and sonicated for 1 h prior to use in an ultrasonic bath. DHLA-QDs were added to a final concentration of 10 nm to the PAH solution under sonication for 5−7 min with intermittent mixing and vortexing, and then left under mild shaking for 1 h in the dark. Both the QDs and polyelectrolytes were precipitated by the addition of excess isopropyl alcohol (IPA) and collected by centrifugation at 10 000 RCF for 15 min at room temperature in a Beckman Coulter Allegra 64 centrifuge and F0685 rotor. The sediment was dissolved in a small amount of pH 7.2−8 Tris and ultracentrifuged overnight (12 h) at 210 000*g* in a Beckman Coulter Optima Max XP ultracentrifuge and either the MLA-50 rotor with Optiseal tubes or the TLA-50 rotor with polyallomer microfuge tubes. The supernatant was carefully removed, using minimal UV illumination to ensure QD retention. The sediment was resuspended by pipet aspiration in the same pH buffer and the process was repeated for 3 total wash cycles, the second and third centrifuge cycles were 6 and 4 h, respectively. This process was repeated to add the second layer of PAA except the adsorption pH was 6−7.2 and the centrifugation pH was 8−8.5.

Conflict of Interest: The authors declare no competing financial interest.

Supporting Information Available: Four graphs are included (luminescence intensity and particle size for different coatings). Additionally, a zoomed in version of Figure 4B, more clearly illustrating PAA pH dependent luminescence intensity and two TEM images showing individual and aggregated QDs are included. This material is available free of charge *via* the Internet at http://pubs.acs.org.

Acknowledgment. This material is based upon work supported by the National Science Foundation under Grant No. (1066928). Use of the TAMU Materials Characterization Facility is acknowledged. Use of TAMU Microscopy and Imaging Center for assistance in acquiring TEM images is acknowledged.

REFERENCES AND NOTES

1. Medintz, I. L.; Uyeda, H. T.; Goldman, E. R.; Mattoussi, H. Quantum Dot Bioconjugates for Imaging, Labelling and Sensing. *Nat. Mater.* **2005**, *4*, 435–446.
2. Petryayeva, E.; Algar, W. R.; Medintz, I. L. Quantum Dots in Bioanalysis: A Review of Applications Across Various

Platforms for Fluorescence Spectroscopy and Imaging. *Appl. Spectrosc.* **2013**, *67*, 215–252.
3. Michalet, X.; Pinaud, F. F.; Bentolila, L. A.; Tsay, J. M.; Doose, S.; Li, J. J.; Sundaresan, G.; Wu, A. M.; Gambhir, S. S.; Weiss, S. Quantum Dots for Live Cells, *in Vivo* Imaging, and Diagnostics. *Science* **2005**, *307*, 538–544.
4. Wu, X. Y.; Liu, H. J.; Liu, J. Q.; Haley, K. N.; Treadway, J. A.; Larson, J. P.; Ge, N. F.; Peale, F.; Bruchez, M. P. Immunofluorescent Labeling of Cancer Marker Her2 and Other Cellular Targets with Semiconductor Quantum Dots. *Nat. Biotechnol.* **2003**, *21*, 41–46.
5. Jaiswal, J. K.; Simon, S. M. Potentials and Pitfalls of Fluorescent Quantum Dots for Biological Imaging. *Trends Cell Biol.* **2004**, *14*, 497–504.
6. Clapp, A. R.; Medintz, I. L.; Mattoussi, H. Forster Resonance Energy Transfer Investigations Using Quantum-Dot Fluorophores. *ChemPhysChem* **2006**, *7*, 47–57.
7. Clapp, A. R.; Medintz, I. L.; Mauro, J. M.; Fisher, B. R.; Bawendi, M. G.; Mattoussi, H. Fluorescence Resonance Energy Transfer Between Quantum Dot Donors and Dye-Labeled Protein Acceptors. *J. Am. Chem. Soc.* **2004**, *126*, 301–310.
8. Clapp, A. R.; Medintz, I. L.; Uyeda, H. T.; Fisher, B. R.; Goldman, E. R.; Bawendi, M. G.; Mattoussi, H. Quantum Dot-Based Multiplexed Fluorescence Resonance Energy Transfer. *J. Am. Chem. Soc.* **2005**, *127*, 18212–18221.
9. Medintz, I. L.; Goldman, E. R.; Lassman, M. E.; Mauro, J. M. A Fluorescence Resonance Energy Transfer Sensor Based on Maltose Binding Protein. *Bioconjugate Chem.* **2003**, *14*, 909–918.
10. Peng, Z. A.; Peng, X. G. Formation of High-Quality CdTe, CdSe, and CdS Nanocrystals Using CdO as Precursor. *J. Am. Chem. Soc.* **2001**, *123*, 183–184.
11. Brichkin, S. B.; Chernykh, E. V. Hydrophilic Semiconductor Quantum Dots. *High Energy Chem.* **2011**, *45*, 1–12.
12. Zhang, Y. J.; Clapp, A. Overview of Stabilizing Ligands for Biocompatible Quantum Dot Nanocrystals. *Sensors* **2011**, *11*, 11036–11055.
13. Sperling, R. A.; Parak, W. J. Surface Modification, Functionalization and Bioconjugation of Colloidal Inorganic Nanoparticles. *Philos. Trans. R. Soc., A* **2010**, *368*, 1333–1383.
14. Zhang, F.; Lees, E.; Amin, F.; Gil, P. R.; Yang, F.; Mulvaney, P.; Parak, W. J. Polymer-Coated Nanoparticles: A Universal Tool for Biolabelling Experiments. *Small* **2011**, *7*, 3113–3127.
15. Zhang, Y. J.; Schnoes, A. M.; Clapp, A. R. Dithiocarbamates as Capping Ligands for Water-Soluble Quantum Dots. *ACS Appl. Mater. Interfaces* **2010**, *2*, 3384–3395.
16. Clapp, A. R.; Goldman, E. R.; Mattoussi, H. Capping of CdSe-ZnS Quantum Dots with DHLA and Subsequent Conjugation with Proteins. *Nat. Protoc.* **2006**, *1*, 1258–1266.
17. Gaponik, N.; Rogach, A. L. Thiol-Capped CdTe Nanocrystals: Progress and Perspectives of the Related Research Fields. *Phys. Chem. Chem. Phys.* **2010**, *12*, 8685–8693.
18. Mattoussi, H.; Mauro, J. M.; Goldman, E. R.; Anderson, G. P.; Sundar, V. C.; Mikulec, F. V.; Bawendi, M. G. Self-Assembly of CdSe-ZnS Quantum Dot Bioconjugates Using an Engineered Recombinant Protein. *J. Am. Chem. Soc.* **2000**, *122*, 12142–12150.
19. Aldana, J.; Wang, Y. A.; Peng, X. G. Photochemical Instability of CdSe Nanocrystals Coated by Hydrophilic Thiols. *J. Am. Chem. Soc.* **2001**, *123*, 8844–8850.
20. Decher, G. Fuzzy Nanoassemblies: Toward Layered Polymeric Multicomposites. *Science* **1997**, *277*, 1232–1237.
21. Decher, G.; Hong, J. D.; Schmitt, J. Buildup of Ultrathin Multilayer Films by a Self-Assembly Process: III. Consecutively Alternating Adsorption of Anionic and Cationic Polyelectrolytes on Charged Surfaces. *Thin Solid Films* **1992**, *210*, 831–835.
22. Sukhorukov, G. B.; Donath, E.; Davis, S.; Lichtenfeld, H.; Caruso, F.; Popov, V. I.; Mohwald, H. Stepwise Polyelectrolyte Assembly on Particle Surfaces: A Novel Approach to Colloid Design. *Polym. Adv. Technol.* **1998**, *9*, 759–767.
23. Gittins, D. I.; Caruso, F. Tailoring the Polyelectrolyte Coating of Metal Nanoparticles. *J. Phys. Chem. B* **2001**, *105*, 6846–6852.
24. Kato, N.; Schuetz, P.; Fery, A.; Caruso, F. Thin Multilayer Films of Weak Polyelectrolytes on Colloid Particles. *Macromolecules* **2002**, *35*, 9780–9787.
25. Dorris, A.; Rucareanu, S.; Reven, L.; Barrett, C. J.; Lennox, R. B. Preparation and Characterization of Polyelectrolyte-Coated Gold Nanoparticles. *Langmuir* **2008**, *24*, 2532–2538.
26. Schneider, G.; Decher, G. Functional Core/Shell Nanoparticles *via* Layer-by-Layer Assembly. Investigation of the Experimental Parameters for Controlling Particle Aggregation and for Enhancing Dispersion Stability. *Langmuir* **2008**, *24*, 1778–1789.
27. Schneider, G.; Decher, G. From Functional Core/Shell Nanoparticles Prepared *via* Layer-by-Layer Deposition to Empty Nanospheres. *Nano Lett.* **2004**, *4*, 1833–1839.
28. Gittins, D. I.; Caruso, F. Multilayered Polymer Nanocapsules Derived from Gold Nanoparticle Templates. *Adv. Mater.* **2000**, *12*, 1947–1949.
29. Mayya, K. S.; Schoeler, B.; Caruso, F. Preparation and Organization of Nanoscale Polyelectrolyte-Coated Gold Nanoparticles. *Adv. Funct. Mater.* **2003**, *13*, 183–188.
30. Hong, X.; Li, J.; Wang, M. J.; Xu, J. J.; Guo, W.; Li, J. H.; Bai, Y. B.; Li, T. J. Fabrication of Magnetic Luminescent Nanocomposites by a Layer-by-Layer Self-Assembly Approach. *Chem. Mater.* **2004**, *16*, 4022–4027.
31. Caruso, F.; Schuler, C.; Kurth, D. G. Core-Shell Particles and Hollow Shells Containing Metallo-Supramolecular Components. *Chem. Mater.* **1999**, *11*, 3394–3399.
32. Jin, Y. D.; Gao, X. H. Plasmonic Fluorescent Quantum Dots. *Nat. Nanotechnol* **2009**, *4*, 571–576.
33. Jaffar, S.; Nam, K. T.; Khademhosseini, A.; Xing, J.; Langer, R. S.; Belcher, A. M. Layer-by-Layer Surface Modification and Patterned Electrostatic Deposition of Quantum Dots. *Nano Lett.* **2004**, *4*, 1421–1425.
34. Kunze, K. K.; Netz, R. R. Salt-Induced DNA-Histone Complexation. *Phys. Rev. Lett.* **2000**, *85*, 4389–4392.
35. Netz, R. R.; Joanny, J. F. Complexation between a Semiflexible Polyelectrolyte and an Oppositely Charged Sphere. *Macromolecules* **1999**, *32*, 9026–9040.
36. Chapel, J. P.; Berret, J. F. Versatile Electrostatic Assembly of Nanoparticles and Polyelectrolytes: Coating, Clustering and Layer-by-Layer Processes. *Curr. Opin. Colloid Interface Sci.* **2012**, *17*, 97–105.
37. Labouta, H. I.; Schneider, M. Tailor-Made Biofunctionalized Nanoparticles Using Layer-by-Layer Technology. *Int. J. Pharm.* **2010**, *395*, 236–242.
38. Adamczak, M.; Hoel, H. J.; Gaudernack, G.; Barbasz, J.; Szczepanowicz, K.; Warszynski, P. Polyelectrolyte Multilayer Capsules with Quantum Dots for Biomedical Applications. *Colloids Surf., B* **2012**, *90*, 211–216.
39. Ruedas-Rama, M. J.; Hall, E. A. H. Multiplexed Energy Transfer Mechanisms in a Dual-Function Quantum Dot for Zinc and Manganese. *Analyst* **2009**, *134*, 159–169.
40. Ruedas-Rama, M. J.; Hall, E. A. H. A Quantum Dot-Lucigenin Probe for Cl^-. *Analyst* **2008**, *133*, 1556–1566.
41. Ruedas-Rama, M. J.; Orte, A.; Hall, E. A. H.; Alvarez-Pez, J. M.; Talavera, E. M. Effect of Surface Modification on Semiconductor Nanocrystal Fluorescence Lifetime. *ChemPhysChem* **2011**, *12*, 919–929.
42. Velapoldi, R. A.; Tonnesen, H. H. Corrected Emission Spectra and Quantum Yields for a Series of Fluorescent Compounds in the Visible Spectral Region. *J. Fluoresc.* **2004**, *14*, 465–472.
43. Byrne, S. J.; Corr, S. A.; Rakovich, T. Y.; Gun'ko, Y. K.; Rakovich, Y. P.; Donegan, J. F.; Mitchell, S.; Volkov, Y. Optimisation of the Synthesis and Modification of CdTe Quantum Dots for Enhanced Live Cell Imaging. *J. Mater. Chem.* **2006**, *16*, 2896–2902.
44. Ruedas-Rama, M. J.; Orte, A.; Hall, E. A. H.; Alvarez-Pez, J. M.; Talavera, E. M. Quantum Dot Photoluminescence Lifetime-Based pH Nanosensor. *Chem. Commun.* **2011**, *47*, 2898–2900.
45. Zhang, H.; Zhou, Z.; Yang, B.; Gao, M. Y. The Influence of Carboxyl Groups on the Photoluminescence of Mercaptocarboxylic Acid-Stabilized CdTe Nanoparticles. *J. Phys. Chem. B* **2003**, *107*, 8–13.

46. Hardzei, M.; Artemyev, M. Influence of pH on Luminescence from Water-Soluble Colloidal Mn-Doped ZnSe Quantum Dots Capped with Different Mercaptoacids. *J. Lumin.* **2012**, *132*, 425–428.
47. Liu, Y. S.; Sun, Y. H.; Vernier, P. T.; Liang, C. H.; Chong, S. Y. C.; Gundersen, M. A. pH-Sensitive Photoluminescence of CdSe/ZnSe/ZnS Quantum Dots in Human Ovarian Cancer Cells. *J. Phys. Chem. C* **2007**, *111*, 2872–2878.
48. Majithia, R.; Patterson, J.; Bondos, S. E.; Meissner, K. E. On the Design of Composite Protein-Quantum Dot Biomaterials *via* Self-Assembly. *Biomacromolecules* **2011**, *12*, 3629–3637.
49. Zylstra, J.; Amey, J.; Miska, N. J.; Pang, L. S.; Hine, C. R.; Langer, J.; Doyle, R. P.; Maye, M. M. A Modular Phase Transfer and Ligand Exchange Protocol for Quantum Dots. *Langmuir* **2011**, *27*, 4371–4379.